



KEK Preprint 2001-63
Belle Preprint 2001-11

Measurement of the Branching Fraction for $B \rightarrow \eta' K$ and Search for $B \rightarrow \eta' \pi^+$

The Belle Collaboration

K. Abe⁹, K. Abe³⁸, R. Abe²⁸, I. Adachi⁹, Byoung Sup Ahn¹⁶, H. Aihara⁴⁰,
M. Akatsu²¹, Y. Asano⁴⁵, T. Aso⁴⁴, V. Aulchenko², A. M. Bakich³⁶,
E. Banas²⁶, S. Behari⁹, P. K. Behera⁴⁶, D. Beilina², A. Bondar², A. Bozek²⁶,
T. E. Browder⁸, B. C. K. Casey⁸, P. Chang²⁵, Y. Chao²⁵, B. G. Cheon³⁵,
R. Chistov¹⁴, S.-K. Choi⁷, Y. Choi³⁵, L. Y. Dong¹², J. Dragic¹⁹,
S. Eidelman², Y. Enari²¹, F. Fang⁸, H. Fujii⁹, C. Fukunaga⁴²,
M. Fukushima¹¹, N. Gabyshev⁹, A. Garmash^{2,9}, T. Gershon⁹, A. Gordon¹⁹,
K. Gotow⁴⁷, R. Guo²³, J. Haba⁹, H. Hamasaki⁹, K. Hara³⁰, T. Hara³⁰,
N. C. Hastings¹⁹, H. Hayashii²², M. Hazumi³⁰, E. M. Heenan¹⁹, I. Higuchi³⁹,
T. Higuchi⁴⁰, H. Hirano⁴³, T. Hojo³⁰, Y. Hoshi³⁸, K. Hoshina⁴³, S. R. Hou²⁵,
W.-S. Hou²⁵, S.-C. Hsu²⁵, H.-C. Huang²⁵, Y. Igarashi⁹, T. Iijima⁹, H. Ikeda⁹,
K. Inami²¹, A. Ishikawa²¹, H. Ishino⁴¹, R. Itoh⁹, G. Iwai²⁸, H. Iwasaki⁹,
Y. Iwasaki⁹, D. J. Jackson³⁰, P. Jalocha²⁶, H. K. Jang³⁴, J. Kaneko⁴¹,
J. H. Kang⁴⁹, J. S. Kang¹⁶, N. Katayama⁹, H. Kawai³, H. Kawai⁴⁰,
N. Kawamura¹, T. Kawasaki²⁸, H. Kichimi⁹, D. W. Kim³⁵, Heejong Kim⁴⁹,
H. J. Kim⁴⁹, Hyunwoo Kim¹⁶, S. K. Kim³⁴, T. H. Kim⁴⁹, K. Kinoshita⁵,
S. Kobayashi³³, H. Konishi⁴³, P. Krokovny², R. Kulasiri⁵, S. Kumar³¹,
A. Kuzmin², Y.-J. Kwon⁴⁹, J. S. Lange⁶, G. Leder¹³, S. H. Lee³⁴,
D. Liventsev¹⁴, R.-S. Lu²⁵, T. Matsubara⁴⁰, S. Matsumoto⁴,
T. Matsumoto²¹, J. MacNaughton¹³, Y. Mikami³⁹, K. Miyabayashi²²,
H. Miyake³⁰, H. Miyata²⁸, G. R. Moloney¹⁹, S. Mori⁴⁵, T. Mori⁴,
A. Murakami³³, T. Nagamine³⁹, Y. Nagasaka¹⁰, Y. Nagashima³⁰,
T. Nakadaira⁴⁰, E. Nakano²⁹, M. Nakao⁹, J. W. Nam³⁵, S. Narita³⁹,
Z. Natkaniec²⁶, K. Neichi³⁸, S. Nishida¹⁷, O. Nitoh⁴³, S. Noguchi²²,
T. Nozaki⁹, S. Ogawa³⁷, T. Ohshima²¹, T. Okabe²¹, S. Okuno¹⁵, H. Ozaki⁹,

arXiv:hep-ex/0108010v1 6 Aug 2001

P. Pakhlov¹⁴, H. Palka²⁶, C. S. Park³⁴, C. W. Park¹⁶, H. Park¹⁸,
L. S. Peak³⁶, M. Peters⁸, L. E. Piiilonen⁴⁷, E. Prebys³², J. L. Rodriguez⁸,
N. Root², M. Rozanska²⁶, K. Rybicki²⁶, H. Sagawa⁹, Y. Sakai⁹,
H. Sakamoto¹⁷, M. Satapathy⁴⁶, A. Satpathy^{9,5}, S. Semenov¹⁴, K. Senyo²¹,
M. E. Sevier¹⁹, H. Shibuya³⁷, B. Shwartz², S. Stanič⁴⁵, A. Sugi²¹,
A. Sugiyama²¹, K. Sumisawa⁹, T. Sumiyoshi⁹, K. Suzuki³, S. Suzuki⁴⁸,
S. Y. Suzuki⁹, S. K. Swain⁸, T. Takahashi²⁹, M. Takita³⁰, K. Tamai⁹,
N. Tamura²⁸, J. Tanaka⁴⁰, M. Tanaka⁹, Y. Tanaka²⁰, Y. Teramoto²⁹,
M. Tomoto⁹, T. Tomura⁴⁰, S. N. Tovey¹⁹, K. Trabelsi⁸, T. Tsuboyama⁹,
T. Tsukamoto⁹, S. Uehara⁹, K. Ueno²⁵, Y. Unno³, S. Uno⁹, Y. Ushiroda⁹,
K. E. Varvell³⁶, C. C. Wang²⁵, C. H. Wang²⁴, J. G. Wang⁴⁷, M.-Z. Wang²⁵,
Y. Watanabe⁴¹, E. Won³⁴, B. D. Yabsley⁹, Y. Yamada⁹, M. Yamaga³⁹,
A. Yamaguchi³⁹, Y. Yamashita²⁷, M. Yamauchi⁹, S. Yanaka⁴¹, J. Yashima⁹,
K. Yoshida²¹, Y. Yusa³⁹, H. Yuta¹, C. C. Zhang¹², J. Zhang⁴⁵, H. W. Zhao⁹,
Y. Zheng⁸, V. Zhilich², and D. Žontar⁴⁵

¹*Aomori University, Aomori*

²*Budker Institute of Nuclear Physics, Novosibirsk*

³*Chiba University, Chiba*

⁴*Chuo University, Tokyo*

⁵*University of Cincinnati, Cincinnati OH*

⁶*University of Frankfurt, Frankfurt*

⁷*Gyeongsang National University, Chinju*

⁸*University of Hawaii, Honolulu HI*

⁹*High Energy Accelerator Research Organization (KEK), Tsukuba*

¹⁰*Hiroshima Institute of Technology, Hiroshima*

¹¹*Institute for Cosmic Ray Research, University of Tokyo, Tokyo*

¹²*Institute of High Energy Physics, Chinese Academy of Sciences, Beijing*

¹³*Institute of High Energy Physics, Vienna*

¹⁴*Institute for Theoretical and Experimental Physics, Moscow*

¹⁵*Kanagawa University, Yokohama*

¹⁶*Korea University, Seoul*

¹⁷*Kyoto University, Kyoto*

¹⁸*Kyungpook National University, Taegu*

¹⁹*University of Melbourne, Victoria*

²⁰*Nagasaki Institute of Applied Science, Nagasaki*

²¹*Nagoya University, Nagoya*

²²*Nara Women's University, Nara*

²³*National Kaohsiung Normal University, Kaohsiung*

²⁴*National Lien-Ho Institute of Technology, Miao Li*

²⁵*National Taiwan University, Taipei*

²⁶*H. Niewodniczanski Institute of Nuclear Physics, Krakow*

²⁷*Nihon Dental College, Niigata*

- ²⁸*Niigata University, Niigata*
²⁹*Osaka City University, Osaka*
³⁰*Osaka University, Osaka*
³¹*Panjab University, Chandigarh*
³²*Princeton University, Princeton NJ*
³³*Saga University, Saga*
³⁴*Seoul National University, Seoul*
³⁵*Sungkyunkwan University, Suwon*
³⁶*University of Sydney, Sydney NSW*
³⁷*Toho University, Funabashi*
³⁸*Tohoku Gakuin University, Tagajo*
³⁹*Tohoku University, Sendai*
⁴⁰*University of Tokyo, Tokyo*
⁴¹*Tokyo Institute of Technology, Tokyo*
⁴²*Tokyo Metropolitan University, Tokyo*
⁴³*Tokyo University of Agriculture and Technology, Tokyo*
⁴⁴*Toyama National College of Maritime Technology, Toyama*
⁴⁵*University of Tsukuba, Tsukuba*
⁴⁶*Utkal University, Bhubaneswer*
⁴⁷*Virginia Polytechnic Institute and State University, Blacksburg VA*
⁴⁸*Yokkaichi University, Yokkaichi*
⁴⁹*Yonsei University, Seoul*

Abstract

We report measurements for two-body charmless hadronic B decays with an η' meson in the final state. Using 11.1×10^6 $B\bar{B}$ pairs collected with the Belle detector, we find $BF(B^+ \rightarrow \eta' K^+) = (79_{-11}^{+12} \pm 9) \times 10^{-6}$ and $BF(B^0 \rightarrow \eta' K^0) = (55_{-16}^{+19} \pm 8) \times 10^{-6}$, where the first and second errors are statistical and systematic, respectively. No signal is observed in the mode $B^+ \rightarrow \eta' \pi^+$, and we set a 90% confidence level upper limit of $BF(B^+ \rightarrow \eta' \pi^+) < 7 \times 10^{-6}$. The CP asymmetry in $B^\pm \rightarrow \eta' K^\pm$ decays is investigated and a limit at 90% confidence level of $-0.20 < A_{CP} < 0.32$ is obtained.

PACS: 13.25.Hw, 14.40.Nd

Charmless hadronic B decays provide a rich ground for studying the mechanisms of B meson decay and the phenomenon of CP violation. The decay $B \rightarrow \eta'K$ is an example of such a charmless decay with an unexpectedly large branching fraction [1]. Within the framework of the Standard Model, the $B \rightarrow \eta'K$ decay proceeds primarily through $b \rightarrow s$ penguin diagrams with a contribution from the $b \rightarrow u$ tree diagram. Recent theory calculations [2,3] underestimate the measured decay rate [4] published by the CLEO collaboration. If the large branching fraction persists after more precise measurements, we will likely need an additional SU(3)-singlet contribution [5] or new physics beyond the Standard Model to explain it. Moreover, if the unitarity triangle angle ϕ_3 (or γ), defined by $\arg(\frac{V_{ub}^*V_{ud}}{-V_{cb}^*V_{cd}})$, is greater than 90 degrees, as suggested from interpretations of $B \rightarrow K\pi, \pi\pi$ results [6,7] under the factorization assumption, $B^+ \rightarrow \eta'K^+$ will be enhanced relative to $B^0 \rightarrow \eta'K^0$ [2,8]. Although expected to be small [9], it is also of interest to examine the direct CP asymmetry in $B^\pm \rightarrow \eta'K^\pm$ decays since new physics may contribute.

In this paper we report on measurements of the branching fractions of B mesons decaying to $\eta'K^+, \eta'\pi^+$, and $\eta'K^0$ final states, where only the $K_S^0 \rightarrow \pi^+\pi^-$ transition is considered for K^0 . Inclusion of charge conjugate modes is implied unless explicitly stated otherwise. The results are obtained from data collected by the Belle detector [10] at the KEKB asymmetric e^+e^- storage ring [11]. The data sample corresponds to an integrated luminosity of 10.4 fb^{-1} and consists of 11.1 million $B\bar{B}$ pairs at the $\Upsilon(4S)$ resonance. The branching fractions are calculated assuming that B^+B^- and $B^0\bar{B}^0$ are produced equally.

A detailed description of the Belle detector can be found in Ref. [10]; here we only describe briefly the parts used in this analysis. Charged tracks are reconstructed inside a 1.5 T solenoidal magnet with a three layer double-sided silicon vertex detector (SVD) and a central drift chamber (CDC) that consists of 50 layers segmented into 6 axial and 5 stereo superlayers. The CDC covers the polar angle range between 17° and 150° in the laboratory frame and, together with the SVD, gives a transverse momentum resolution of $(\sigma_{p_t}/p_t)^2 = (0.0019 p_t)^2 + (0.0030)^2$, where p_t and σ_{p_t} are in GeV/ c . Charged kaon and pion identification is performed using a combination of three devices: an array of 1188 aerogel Čerenkov counters (ACC) covering the momentum range 1–4 GeV/ c , a time-of-flight scintillation counter system (TOF) for track momenta below 1.5 GeV/ c , and dE/dx information from the CDC for particles with very low or high momenta. Situated between these devices and the solenoid coil is an electromagnetic calorimeter (ECL) consisting of 8736 CsI(T ℓ) crystals with typical cross-section of $5.5 \times 5.5 \text{ cm}^2$ at the front surface and a depth of $16.2 X_0$. The ECL provides a photon energy resolution of $(\sigma_E/E)^2 = 0.013^2 + (0.0007/E)^2 + (0.008/E^{1/4})^2$, where E and σ_E are in GeV.

Charged tracks are required to come from the collision point and have transverse momenta p_t above 100 MeV/ c . These charged tracks are then refitted

with their vertex position constrained to the run-averaged profile of B meson decay vertices in the transverse plane. For $\eta' \rightarrow \rho^0\gamma$ decays, in order to reduce backgrounds, the minimum p_t requirement is increased to 200 MeV/ c .

Charged K and π mesons coming directly from two-body B decays are identified by combining K/π probabilities from the CDC (dE/dx) and the ACC to form a $K(\pi)$ likelihood $L_K(L_\pi)$. As these mesons have momenta above 1.5 GeV/ c in the laboratory frame, TOF information does not provide any discrimination. Discrimination between kaons and pions is then achieved through the likelihood ratio, $L_K/(L_\pi + L_K)$. The performance of hadron identification is studied using a high momentum D^{*+} data sample, where $D^{*+} \rightarrow D^0\pi^+$, $D^0 \rightarrow K^-\pi^+$. Selected K and π tracks are required to be in the same kinematic region as those from two-body B decays. We measure the pion and kaon identification efficiencies to be $(92.4 \pm 2.4)\%$ and $(84.9 \pm 2.1)\%$, respectively. The rate for true pions to be misidentified as kaons is $(4.3 \pm 0.4)\%$ while the rate for true kaons to be misidentified as pions is $(10.4 \pm 0.6)\%$. For charged pions from η' decays, tracks identified to be highly kaon-like (including TOF information) are rejected. This loose kaon rejection requirement is studied using $K_S^0 \rightarrow \pi^+\pi^-$ events. The typical efficiency for charged pions is $(98.2 \pm 1.0)\%$. K_S^0 candidates are reconstructed by constraining a pair of oppositely charged tracks with a common vertex. This vertex is required to be distinct from the collision point and consistent with the K_S^0 flight direction. The invariant mass is required to be within ± 30 MeV/ c^2 of the nominal K_S^0 mass.

Two channels have been used for η' reconstruction: $\eta' \rightarrow \eta\pi^+\pi^-$, $\eta \rightarrow \gamma\gamma$ and $\eta' \rightarrow \rho^0\gamma$. Candidate photons from η (η') decays are required to be isolated and have energies exceeding 50 (100) MeV. To reject soft photon backgrounds, $\eta \rightarrow \gamma\gamma$ candidates are selected with $|\cos\theta^*| < 0.97$, where θ^* is the angle between the photon direction in the η rest frame and the η momentum. The momenta of η candidates with invariant mass between 500 and 570 MeV/ c^2 are recalculated by applying an η mass constraint. We require $\pi^+\pi^-$ pairs from the $\eta' \rightarrow \rho^0\gamma$ decay to be two oppositely charged tracks having an invariant mass between 550 and 920 MeV/ c^2 . Fig. 1 shows the mass distributions for η' candidates. The reconstructed mass resolutions are 12 MeV/ c^2 for $\eta \rightarrow \gamma\gamma$, 2.7 MeV/ c^2 for $\eta' \rightarrow \eta\pi^+\pi^-$, and 8.8 MeV/ c^2 for $\eta' \rightarrow \rho^0\gamma$. Candidate η' mesons are required to have a reconstructed mass within 3σ of the nominal η' mass.

Candidate B mesons are identified using the beam constrained mass $M_{bc} = \sqrt{E_{\text{beam}}^2 - P_B^2}$ and the energy difference $\Delta E = E_B - E_{\text{beam}}$, where $E_{\text{beam}} = 5.29$ GeV, and P_B and E_B are the momentum and energy of a B candidate in the $\Upsilon(4S)$ rest frame. In the $B^+ \rightarrow \eta' h^+$ ($h = K, \pi$) study, E_B is computed with a kaon mass hypothesis for h^+ , which results in a shift of +44 MeV in ΔE for $\eta'\pi^+$ events. This shift in ΔE provides additional discrimination between the $\eta'K^+$ and $\eta'\pi^+$ final states. The parameterizations of the signal in M_{bc} and ΔE

are determined by a GEANT [12] based Monte Carlo (MC) simulation and verified using a sample of $B^+ \rightarrow \bar{D}^0 \pi^+$, $\bar{D}^0 \rightarrow K^+ \pi^- \pi^0$ events. The Gaussian width of the signal in M_{bc} is about $2.9 \text{ MeV}/c^2$, and mainly comes from the beam energy spread. The ΔE distribution is found to be slightly asymmetric with a small tail on the lower side due to γ interactions with material in front of the calorimeter and shower leakage out of the back side of the crystals. This ΔE distribution is modeled by a sum of two Gaussians, one of which is asymmetric. The signal region is defined as $M_{bc} > 5.27 \text{ GeV}/c^2$ and $-0.10 \text{ GeV} < \Delta E < 0.08 \text{ GeV}$. Events located in the region $M_{bc} < 5.265 \text{ GeV}/c^2$ are defined as sideband events and are used for background studies. Events with $M_{bc} > 5.2 \text{ GeV}/c^2$ and $|\Delta E| < 250 \text{ MeV}$ are selected for the final analysis.

The dominant background for two-body B decay events comes from the $e^+e^- \rightarrow q\bar{q}$ continuum. In order to reduce this background, several shape variables are chosen to distinguish spherical $B\bar{B}$ events from jet-like continuum events. The variable θ_T is defined as the angle between the candidate η' direction and the thrust axis formed by the momenta of particles not from the B candidate. The continuum background, which accumulates mainly very near $|\cos \theta_T| = 1.0$, is first reduced by requiring $|\cos \theta_T| < 0.9$. Two other variables used are θ_B , the angle between the B flight direction and the beam axis, and S_\perp [13], the scalar sum of the transverse momenta of all particles outside a 45° cone around the candidate η' direction divided by the scalar sum of their momenta. Furthermore, we introduce a set of variables inspired from the Fox-Wolfram moments [14], defined as:

$$R_l^{so} = \frac{\sum_{i,k} |\vec{p}_i| |\vec{p}_k| P_l(\cos \theta_{ik})}{\sum_{i,k} |\vec{p}_i| |\vec{p}_k|}, \quad R_l^{oo} = \frac{\sum_{i,j} |\vec{p}_i| |\vec{p}_j| P_l(\cos \theta_{ij})}{\sum_{i,j} |\vec{p}_i| |\vec{p}_j|},$$

where \vec{p} indicates particle momentum, P_l is the Legendre polynomial of l th order, k is either η' or h from the B candidate, and i, j enumerate all remaining photons and charged particles in the event. Since R_1^{so} , R_3^{so} , and R_1^{oo} are found to be correlated with M_{bc} , we do not use them. We combine the other five variables ($l \leq 4$) together with $\cos \theta_T$ and S_\perp to form a Fisher discriminant F ,

$$F = \sum_{l=2,4} \alpha_l R_l^{so} + \sum_{l=2,3,4} \beta_l R_l^{oo} + c_1 |\cos \theta_T| + c_2 S_\perp,$$

where α_l , β_l , c_1 and c_2 are determined by optimizing the separation between $B\bar{B}$ events and continuum events. For the channel with $\rho\gamma$ in the final state, additional discrimination is gained by using the helicity variable H , which is the cosine of the angle between the π^+ momentum direction in the ρ rest frame and the ρ momentum direction in the η' rest frame. Although there is a small non-resonant contribution in the $\eta' \rightarrow \pi^+ \pi^- \gamma$ process, experimental data [15] indicate that the helicity distribution can still be described by $1 - H^2$.

The variables $\cos\theta_B$, F and H (for the $\rho\gamma$ channel) are found to be independent. The probability density functions (PDF) for these variables are obtained using MC simulations for signal, and sideband events for $q\bar{q}$ background (see Fig. 2). These variables are then combined to form a likelihood ratio $LR = L_s/(L_s + L_{q\bar{q}})$, where $L_{s(q\bar{q})}$ is the product of signal ($q\bar{q}$) probability densities. Since each channel has a different background, we optimize the LR requirement mode by mode by studying the signal significance ($N_S/\sqrt{N_S + N_B}$) using both MC and data samples, where N_S and N_B are signal yields and background yields, respectively. For instance, a loose LR requirement ($LR > 0.4$) for the $\eta\pi^+\pi^-$ mode keeps 83% of the $\eta'K^+$ signal and reduces 74% of the background, while for the $\rho\gamma$ mode a tighter requirement ($LR > 0.6$) is used with a signal efficiency of 70% and a background rejection of 88%. The effect of these requirements is studied by comparing $B^+ \rightarrow \bar{D}^0\pi^+$ in data and MC with different values of LR . The background from $b \rightarrow c$ transitions is negligible as determined by MC study.

Fig. 3 shows the M_{bc} and ΔE distributions for the combined $\eta\pi\pi$ and $\rho\gamma$ samples (and $\eta\pi\pi$ separately) in the $\eta'K^+$, $\eta'\pi^+$ and $\eta'K_S^0$ decay modes. Events in the M_{bc} (ΔE) plots are required to be in the ΔE (M_{bc}) signal region after all selection criteria are applied. Clear signal peaks appear in both the $\eta'K^+$ and $\eta'K_S^0$ channels. The M_{bc} and ΔE distributions in each sample are fitted simultaneously with signal and background functions using an extended unbinned maximum likelihood fit. For N input candidates, the likelihood is defined as

$$L(N_S, N_B) = \frac{e^{-(N_S+N_B)}}{N!} \prod_{i=1}^N [N_S P_{S_i}(M_{bc}, \Delta E) + N_B P_{B_i}(M_{bc}, \Delta E)],$$

where P_{S_i} and P_{B_i} are the probability densities for event i to be signal and background for variables M_{bc} and ΔE , respectively. In the extended maximum likelihood (ML) fit, the extracted yields for signal (N_S) and for background (N_B) are considered separately to follow the Poisson statistics. In this definition, the sum of N_S and N_B equals the number of input candidates N when the likelihood is maximized. The M_{bc} background shape is modeled with a smooth function [16] with parameters determined using events outside of the ΔE signal region. The ΔE background shape is modeled by a linear function with the slope determined from the sideband data and cross-checked using MC events. Since significant signal peaks are observed in the $\eta'K^+$ channel, we can expect contamination in the $\eta'\pi^+$ signal region from $\eta'K^+$. Therefore, an $\eta'K^+$ signal shape is added in the ΔE PDF for $\eta'\pi^+$. The final signal yields are then obtained by this two dimensional (2-D) fit with the statistical significance (Σ) defined as $\sqrt{-2 \ln(L_0/L_{\max})}$, where L_0 and L_{\max} denote the likelihood values at zero signal events and the best fit numbers, respectively. The second and third columns of Table 1 list the fit yields and their significances.

The systematic error for the signal yield is estimated by varying each parameter of the fit functions by $\pm 1\sigma$ from the measured values. The shifts in signal yield are then added in quadrature. In order to study intrusions into the signal regions from other rare B decays, a large MC sample of all known rare B decay processes has been generated. No significant contributions are found.

Signal efficiencies are first obtained using MC simulations and corrected by comparing data and MC predictions for other processes. The tracking efficiency is studied using high momentum D , η and $K^*(892)$ samples. The $\gamma\gamma$ reconstruction efficiency is verified by measuring the branching ratio of two D^0 decay channels, $D^0 \rightarrow K^-\pi^+\pi^0$ to $D^0 \rightarrow K^-\pi^+$, and four $K^*(892)$ decay channels, $K^+\pi^-$, $K^+\pi^0$, $K_S^0\pi^+$, and $K_S^0\pi^0$. The simulation of low momentum photons is further tested by comparing the decay angular distribution of η for data with MC predictions. The systematic errors on the charged track reconstruction efficiencies of $\eta' \rightarrow \eta\pi^+\pi^-$ and $\eta' \rightarrow \rho\gamma$ are estimated by comparing the ratio of $\eta \rightarrow \pi^+\pi^-\pi^0$ to $\eta \rightarrow \gamma\gamma$ in data with MC expectations. The reconstruction of high momentum K_S^0 is studied using the ratio of $D^+ \rightarrow K_S^0\pi^+$ to $D^+ \rightarrow K^-\pi^+\pi^+$. The final systematic errors, including contributions from reconstruction efficiency, hadron identification and 2-D fits, are estimated to be 12% for the $\eta'K^+$ and $\eta'\pi^+$ modes, and 15% for the $\eta'K_S^0$ mode.

Table 1 summarizes the fit results for each reconstructed decay channel. The systematic errors for the branching fractions combine the above systematic errors with that from the number of $B\bar{B}$ events. Results from the $\eta\pi^+\pi^-$ and $\rho\gamma$ channels are then combined by adding the $-2\ln L(BF)$ functions of branching fractions with approximating $N = N_S + N_B$ and extracting the values and 1σ deviations at maximum $L(BF)$. Since no significant signal is seen in the $\eta'\pi^+$ mode, a 90% confidence level (C.L.) upper limit is given by finding the branching fraction that corresponds to 90% of the integral of $L(BF)$. The final upper limit is then computed by adding one standard deviation of the systematic error. The final branching fractions, significance, upper limit, and theoretical predictions are listed in Table 2. With 11.1 million $B\bar{B}$ events, we measure the branching fractions to be $(79_{-11}^{+12} \pm 9) \times 10^{-6}$ for $B^+ \rightarrow \eta'K^+$ and $(55_{-16}^{+19} \pm 8) \times 10^{-6}$ for $B^0 \rightarrow \eta'K^0$. The first errors are statistical and the second systematic. The 90% C.L. upper limit for $B^+ \rightarrow \eta'\pi^+$ is 7×10^{-6} . Our results are consistent with previous measurements given by CLEO [4], but larger than theoretical predictions [2]. The results are also compatible with the preliminary results from BABAR [17]. The upper limit on $\eta'\pi^+$ is currently the most restrictive experimental result.

To study charge asymmetry, the $\eta'K^\pm$ sample is divided into two subsamples: $\eta'K^+$ and $\eta'K^-$. The 2-D fit in the M_{bc} vs. ΔE plane is performed for each subsample. The fitted number of signal events in the $\eta' \rightarrow \eta\pi\pi$, and $\eta' \rightarrow \rho\gamma$ modes are $18.2_{-4.4}^{+5.1}$, and $13.9_{-5.1}^{+6.0}$ for B^+ decays, and $10.7_{-3.4}^{+4.1}$, and $27.9_{-6.2}^{+7.0}$ for B^- decays, respectively. The number of produced B^+ and B^- are obtained

by maximizing the product of the likelihoods for each submode. The number of produced events is 398_{-80}^{+90} for $B^+ \rightarrow \eta' K^+$ and 450_{-88}^{+98} for $B^- \rightarrow \eta' K^-$; the errors are statistical only. The CP asymmetry (A_{CP}) is calculated as $(N(B^-) - N(B^+))/(N(B^-) + N(B^+))$. Since the systematic errors on η' reconstruction and the number of $B\bar{B}$ events cancel in the ratio, the systematic uncertainty of A_{CP} comes mainly from the reconstruction efficiency of charged kaons and the 2-D fit. The asymmetry in the K^\pm efficiency is studied using inclusive charged kaons. The latter is measured by varying the parameters of the fit functions. We find the systematic errors for A_{CP} are 0.01 for K^\pm reconstruction and 0.01 for the 2-D fit [18]. The A_{CP} for the $B^\pm \rightarrow \eta' K^\pm$ decay is finally measured to be $+0.06 \pm 0.15 \pm 0.01$, which corresponds to $-0.20 < A_{CP} < 0.32$ at the 90% confidence level.

In summary, we have searched for charmless hadronic B decays with η' mesons in the final state. Our results confirm that the branching fractions of $B^+ \rightarrow \eta' K^+$ and $B^0 \rightarrow \eta' K^0$ are large. The branching fraction of $B^+ \rightarrow \eta' \pi^+$ is less than 7×10^{-6} at the 90% C.L. With about 70 $B^\pm \rightarrow \eta' K^\pm$ events, no significant charge asymmetry is observed. Our value for $B \rightarrow \eta' K^+$ is somewhat larger than that for $B \rightarrow \eta' K^0$, as predicted under the factorization assumption, but the difference is not statistically significant. If this difference is confirmed with better precision, it will, along with a measurement of time dependent CP asymmetry in $B^0 \rightarrow \eta' K^0$, provide information to understand the underlying dynamics of $B \rightarrow \eta' K$ decays.

We wish to thank the KEK accelerator group for excellent operations. We acknowledge support from the Ministry of Education, Culture, Sports, Science and Technology of Japan and the Japan Society for the Promotion of Science; the Australian Research Council and the Australian Department of Industry, Science and Resources; the Department of Science and Technology of India; the BK21 program of the Ministry of Education of Korea and the Center for High Energy Physics sponsored by the KOSEF; the Polish State Committee for Scientific Research under contract No.2P03B 17017; the Ministry of Science and Technology of Russian Federation; the National Science Council and the Ministry of Education of Taiwan; the Japan-Taiwan Cooperative Program of the Interchange Association; and the U.S. Department of Energy.

References

- [1] CLEO Collaboration, B.H. Behrens *et al.*, Phys. Rev. Lett. **80** (1998) 3710.
- [2] A. Ali, G. Kramer, and C.-D. Lu, Phys. Rev. D **58** (1998) 094009; Y.-H. Chen, H.-Y. Cheng, B. Tseng, and K.-C. Yang, Phys. Rev. D **60** (1999) 094014; H.-Y. Cheng and K.C. Yang, Phys. Rev. D **62** (2000) 054029.

- [3] E. Kou and A.I. Sanda, hep-ph/0106159 (2001).
- [4] CLEO Collaboration, S.J. Richichi *et al.*, Phys. Rev. Lett. **85** (2000) 520.
- [5] H.-Y. Cheng, in Proc. XXXth Int. Conf. on High Energy Phys. (ICHEP2000), edited by C.S. Lim and T. Yamanaka, World Scientific, Singapore (2001).
- [6] CLEO Collaboration, D. Cronin-Hennessy *et al.*, Phys. Rev. Lett. **85** (2000) 515.
- [7] Belle Collaboration, K. Abe *et al.*, Belle preprint 2001-5 (hep-ex/0104030), to be published in Phys. Rev. Lett.
- [8] X.-G. He, W.-S. Hou, and K.-C. Yang, Phys. Rev. Lett. **83** (1999) 1100.
- [9] A. Ali, G. Kramer, and C.-D. Lu, Phys. Rev. D **59** (1999) 014005.
- [10] Belle Collaboration, A. Abashian *et al.*, KEK Progress Report 2000-4 (2000), to be published in Nucl. Inst. and Meth. A.
- [11] KEK accelerator group, KEKB B-Factory Design Report, KEK Report 95-7 (1995), unpublished.
- [12] R. Brun *et al.*, GEANT 3.21, CERN Report No. DD/EE/84-1 (1987).
- [13] CLEO Collaboration, R. Ammar *et al.*, Phys. Rev. Lett. **71** (1993) 674.
- [14] G. Fox and S. Wolfram, Phys. Rev. Lett. **41** (1978) 1581.
- [15] S.I. Bityukov *et al.*, Z. Phys. C **50** (1991) 451; Crystal Barrel Collaboration, A. Abele *et al.*, Phys. Lett. B **402** (1997) 195.
- [16] ARGUS Collaboration, H. Albrecht *et al.*, Phys. Lett. B **241** (1990) 278.
- [17] BABAR Collaboration, T. Champion, in Proc. XXXth Int. Conf. on High Energy Phys. (ICHEP2000), edited by C.S. Lim and T. Yamanaka, World Scientific, Singapore (2001).
- [18] For a more detailed description of the systematic errors in A_{CP} from K^\pm reconstruction, see Belle Collaboration, K. Abe *et al.*, Belle preprint 2001-9 (hep-ex/0106095), to be published in Phys. Rev. D.

Table 1

Summary of results for each channel listed in the first column. The measured signal yield (N_S), statistical significance (Σ), reconstruction efficiency (ϵ), total efficiency including the secondary branching fraction (B_s), and the measured branching fractions are shown. The branching fractions are calculated by assuming that B^+B^- and $B^0\bar{B}^0$ are produced equally from $\Upsilon(4S)$ decays. Uncertainties shown in 2nd and 6th columns are statistical only.

Mode	N_S	Σ	$\epsilon(\%)$	$\epsilon B_s(\%)$	$BF(10^{-6})$
$\eta'_{\eta\pi\pi}K^+$	$28.9^{+6.5}_{-5.7}$	9.4	21.7	3.78	69^{+15}_{-14}
$\eta'_{\rho\gamma}K^+$	$42.5^{+9.1}_{-8.3}$	7.5	14.2	4.18	92^{+20}_{-18}
$\eta'_{\eta\pi\pi}\pi^+$	$0.0^{+1.2}_{-0.0}$	0.0	23.7	4.11	-
$\eta'_{\rho\gamma}\pi^+$	$0.0^{+5.6}_{-0.0}$	0.0	15.4	4.55	-
$\eta'_{\eta\pi\pi}K^0$	$6.4^{+3.4}_{-2.7}$	3.5	20.8	1.25	46^{+25}_{-20}
$\eta'_{\rho\gamma}K^0$	$10.1^{+4.4}_{-3.6}$	4.0	11.5	1.16	79^{+34}_{-28}

Table 2

Combined branching fractions (BF) or 90% C.L. limit, significance (Σ) of Belle, CLEO [4], BABAR [17] and theoretical expectations [2,3]. The branching fractions are in units of 10^{-6} .

Mode	This measurement(BF)	Σ	CLEO	BABAR	Theory
$B^+ \rightarrow \eta'K^+$	$79^{+12}_{-11} \pm 9$	12.0	$80^{+10}_{-9} \pm 7$	$62 \pm 18 \pm 8$	21–53
$B^+ \rightarrow \eta'\pi^+$	< 7	0.0	< 12	-	1–3
$B^0 \rightarrow \eta'K^0$	$55^{+19}_{-16} \pm 8$	5.4	$89^{+18}_{-16} \pm 9$	< 112	20–50

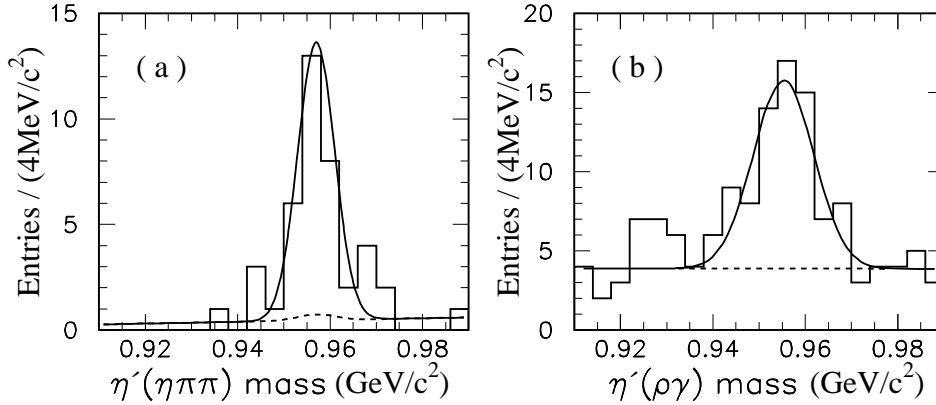


Fig. 1. Reconstructed mass spectra for $\eta' \rightarrow \eta\pi^+\pi^-$ (left) and $\eta' \rightarrow \rho\gamma$ (right) for events in the $M_{bc}-\Delta E$ signal region after applying all analysis requirements.

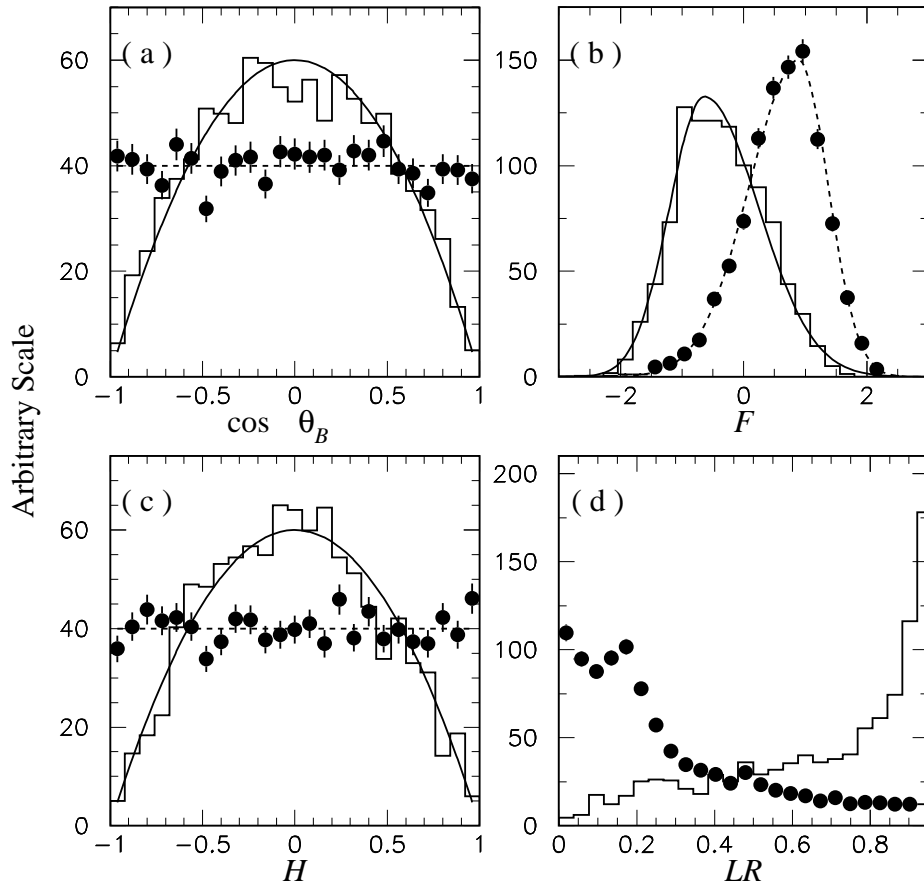


Fig. 2. Event shape distributions for (a) $\cos \theta_B$, (b) F , (c) H and (d) LR for the $\rho\gamma$ mode. Histograms represent the signal distributions (MC), while solid points are from data outside the signal region. Superimposed in (a), (b) and (c) are the PDF parameterizations.

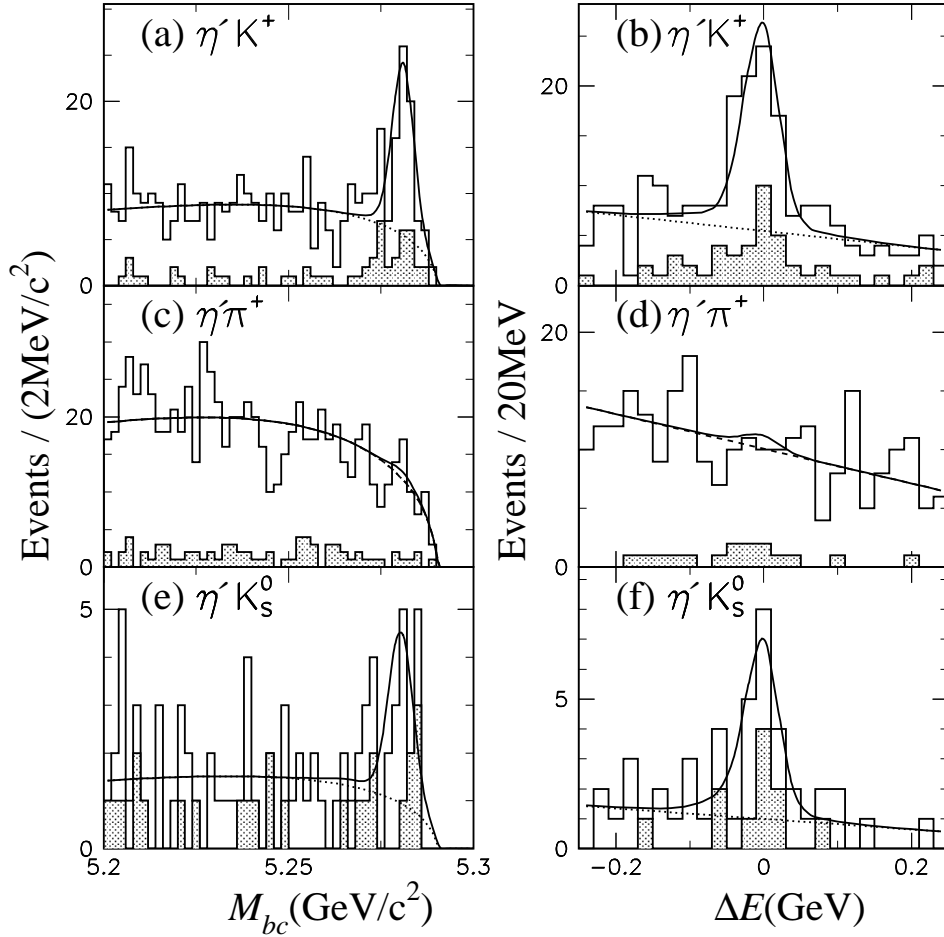


Fig. 3. M_{bc} and ΔE projections for $\eta'K^+$, $\eta'\pi^+$ and $\eta'K_s^0$ events. The shaded histograms correspond to the $\eta' \rightarrow \eta\pi^+\pi^-$ mode while the histograms are for all the modes combined. The superimposed curves show the fits to M_{bc} and ΔE . Solid curves are for signals plus backgrounds and dashed curves are for backgrounds only.

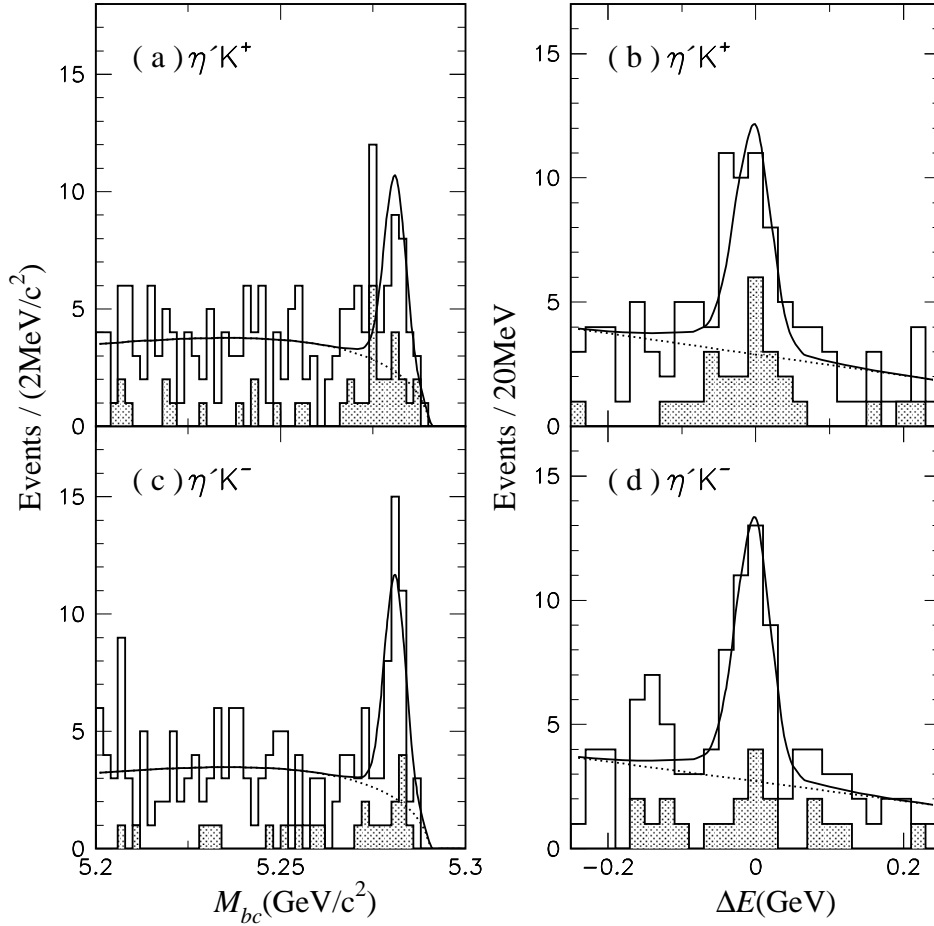


Fig. 4. M_{bc} and ΔE projections for $\eta'K^+$ and $\eta'K^-$ events. The shaded histograms correspond to the $\eta' \rightarrow \eta\pi^+\pi^-$ mode while the histograms are for all the modes combined. The superimposed curves show the fits to M_{bc} and ΔE . Solid curves are for signals plus backgrounds while the dashed curves are for backgrounds only.